Vitreous Cytokine Expression and a Murine Model Suggest a Key Role of Microglia in the Inflammatory Response to Retinal Detachment

Lee Kiang,[1] Bing X. Ross,[2] Jingyu Yao,[2] Sumathi Shanmugam,[2] Chris A. Andrews,[2] Sean Hansen,[2] Cagri G. Besirli,[2] David N. Zacks,[2] and Steven F. Abcouwer[2]

[1]Oregon Health and Science University, Casey Eye Institute, Portland, Oregon, United States
[2]University of Michigan Medicine, Kellogg Eye Center, Ann Arbor, Michigan, United States

Correspondence: Steven F. Abcouwer, Department of Ophthalmology and Visual Sciences, University of Michigan Kellogg Eye Center, 1000 Wall Street, Ann Arbor, MI 48105, USA; sabcouwe@umich.edu.

Submitted: April 2, 2018
Accepted: June 11, 2018

Citation: Kiang L, Ross BX, Yao J, et al. Vitreous cytokine expression and a murine model suggest a key role of microglia in the inflammatory response to retinal detachment. *Invest Ophthalmol Vis Sci*. 2018;59:3767–3778. https://doi.org/10.1167/iovs.18-24489

Purpose. Retinal detachment (RD) separates the retina from the underlying retinal pigment epithelium, resulting in a gradual degeneration of photoreceptor (PR) cells. It is known that RD also results in an inflammatory response, but its contribution to PR degeneration is unknown. In this study we examine the inflammatory responses to RD in patient vitreous and validate a mouse experimental RD as a model of this phenomenon.

Methods. Multiplex bead arrays were used to examine cytokine levels in vitreous samples from 24 patients with macula-off rhegmatogenous retinal detachment (RRD) undergoing reattachment surgery and from 10 control patients undergoing vitrectomy for vitreous opacities or epiretinal membrane. Activation of the innate immune response was then examined in a mouse model of RD.

Results. Twenty-eight factors were significantly increased in vitreous from RD patients versus controls. Notable were the cytokines MCP-1 (CCL2), IP-10 (CXCL10), fractalkine (CX3CL1), GRO (CXCL1), MDC (CCL22), IL-6, and IL-8, which all exhibited relatively high concentrations and several-fold increases in the vitreous of RD patients. Concentrations of various analytes correlated with a range of clinical variables such as duration of detachment and visual acuity. Retinal detachment in the mouse resulted in cytokine mRNA expression changes consistent with human RD vitreous results, as well as microglial proliferation and migration toward the outer retina.

Conclusions. The findings suggest that an inflammatory response involving microglia is a component of the reaction to retinal detachment that may impact visual acuity after surgical repair and that mouse experimental RD can serve as a model to study this effect.

Keywords: inflammation, microglia, leukocytes, retinal detachment

Retinal detachment (RD) describes the separation of neural retina from the retinal pigment epithelium (RPE), which occurs in approximately 1 in 10,000 to 20,000 people per year.[1] Rhegmatogenous RD (RRD) is the most common type of detachment and is characterized by a full-thickness break in the neural retina leading to vitreous fluid influx into the subretinal space. Thus, RRD causes photoreceptor (PR) cells to lose direct contact with the RPE, exposes them to liquid vitreous humor, and forms a diffusional barrier to the flux of oxygen and nutrients coming from the RPE and the choroid vasculature.[2] The resultant hypoxia and nutrient deprivation are evidenced by the upregulation of hypoxia-inducible factors (HIFs) and triggering of autophagy in PR observed in experimental models of RD.[3,4] Such protective mechanisms prevent the rapid death of PR after RD, such that surgical intervention can produce an eventual recovery of good visual acuity (VA) even when reattachment occurs several days after the onset of symptoms.[5] However, the eventual consequence of retina-RPE separation is death of the PR cells, contributing to loss of vision.[6]

RD also leads to the activation of innate immune responses and inflammatory gene expression. Several studies have documented elevated levels of cytokines and growth factors in the vitreous of RD patients.[7–13] Transcriptomic analysis following RD in porcine and human retinas found that inflammatory genes dominated the response.[14,15] Experimental models of RD exhibit increased cytokine expression, gliosis, microgliosis, and subretinal infiltration of monocytes/macrophages.[15–25] Inflammation and high levels of growth factors in the vitreous are two factors thought to contribute to the onset of proliferative vitreoretinopathy (PVR) in patients with RD.[26] PVR, characterized by cellular proliferation and the formation of membranes on the vitreous and subretinal surfaces of the detached retina, is the major cause of poor outcomes in RD surgery.[1] However, the contribution of the innate immune responses and cytokine expression to loss of vision in RD patients without PVR is not well established.

In the present study, multiplex bead array immunoanalysis was used to examine the concentrations of cytokines, growth factors, and soluble receptors in vitreous samples from patients with macula-off primary RRD undergoing surgical repair and from control patients with normal PR cells undergoing vitrectomy for vitreous opacities or epiretinal membrane. Vitreous protein concentrations were compared to clinical covariates to test associations with clinical severity, duration of

detachment, and visual acuities. A mouse model of RD was used to examine the effects of detachment on retinal cytokine mRNA expression, the attraction of leukocytes to the retina following RD, and the response of retinal microglia to RD. The results suggest that RD causes an inflammatory response that positively correlates with extent of detachment and correlates with worse VA after reattachment. In the mouse, RD caused increased expression of several cytokines associated with microglial activation, as well as microglial proliferation and migration toward the distressed PR cells. The findings suggest that an inflammatory response involving microglia is a component of the reaction to RD in humans and a rodent RD model.

Methods

Analysis of Human RD Patients and Controls

A nonrandomized clinical study was performed at the Kellogg Eye Center, University of Michigan, with Institutional Review Board approval, and conformed to the tenets of the Declaration of Helsinki. Twenty-four patients with a primary macula-off RRD that did not develop PVR postoperatively, as well as 10 control patients undergoing vitrectomy for vitreous opacities or epiretinal membrane, were included in the study. Inclusion criterion for the study group was detachment of the retina with macula-off status. For the control group, inclusion criteria were presence of visually significant vitreous opacity or epiretinal membrane with no previous history of RD. Exclusion criteria for the RD group were development of PVR, vitrectomy, or incomplete data on final VA. The clinical information recorded for RD patients included sex, age, preoperative lens status, preoperative best-corrected visual acuity (BCVA), extent of detachment in clock hours (as reported in the clinical exam and operative report), duration of detachment (time from reported onset of symptoms to surgical repair), time of follow-up to exam, postoperative BCVA at follow-up examination, postoperative lens status, and the presence of any concurrent ocular pathology expected to contribute to decreased visual acuity. BCVA was evaluated with a Snellen chart and was converted to logarithm of the minimum angle of resolution (logMAR) value.

Undiluted vitreous was obtained at the time of vitrectomy as previously described.[27] Samples containing 25 μL undiluted vitreous were analyzed using two assay panels with a detection system (Milliplex and Luminex, respectively; Millipore-Sigma, St. Louis, MO, USA) per manufacturer instructions. A total of 47 different analytes were measured. The assays included the Human Cytokine/Chemokine Panel I (panel 1, Cat. No. HCYTMAG-60K-PX41; Millipore-Sigma), which measures 41 analytes, and the Human CD8+ T-Cell Panel (panel 2, Cat. No. HCD8MAG15K17PMX; Millipore-Sigma), which included 17 analytes (see Supplementary Table S2 for a list of analytes and definition of abbreviations). A cutoff of 30 beads was used as a threshold for low bead count, such that assays with fewer than 30 bead counts were treated as missing data. Averages of two technical duplicates were used for analysis. Limits of detection were determined from manufacturer specifications.

Statistical Analysis of Vitreous Analyte Data

For statistical analyses, maximum likelihood estimation was used to fit a log normal distribution to each separate set of RD and control analyte concentrations. Measurements below or above the limits of detection were treated as left-censored or right-censored, respectively. All applied statistical methods are able to incorporate censored data. Analytes were not included in the analyses if more than half of the measurements in a group (RD or control) were below the limit of detection. Equality of mean log concentration for RD and control groups was tested by a Wald test. Additionally, analyte concentrations were regressed on covariates using parametric survival analysis assuming log normality. Control and RD measurements were regressed on sex and age, while only the RD measurements were regressed on extent of detachment, duration of detachment, and logMAR BCVA (preoperative, postoperative, and change). Standard β values were used to show the extent of change in the outcome variable for every unit change in the predictor variable. Duration between onset and surgery was converted to $\log_{10}$(days) for analysis. Nonparametric alternatives were also computed to check robustness to normality assumption. Multivariate structure was investigated with hierarchical cluster analysis of the associations and with principal component analysis using imputed data. All analyses were performed using statistical software (R version 3.3.2; R Foundation for Statistical Computing, Vienna, Austria). P values were not adjusted for multiple comparisons and $\alpha = 0.05$ was considered significant. For more conservative estimates of statistical significance, only P values with a Bonferroni-corrected $\alpha = 0.001$ (0.05/47) can be considered significant.

Mouse RD Model

All animal experiments were approved by the University Committee on Use and Care of Animals at the University of Michigan and were in accordance with the Association for Research in Vision and Ophthalmology Statement for the Use of Animals in Ophthalmic and Visual Research. Retina-RPE separations were created using a transscleral-transvitreal-subretinal injection procedure established in our laboratory[28] based on one originally described by Anderson and colleagues for the cat.[29] The reader is directed to the diagram representing "transscleral subretinal injection for adult mice" within Figure 1 of Qi et al.[30] Adult C57BL6/J mice (Jackson Laboratory, Bar Harbor, ME, USA) aged 8 to 12 weeks were anesthetized with a 1:1 mixture of ketamine (100 mg/mL) and xylazine (20 mg/mL), and pupils were dilated with topical application of 2.5% phenylephrine and 1% tropicamide. A sclerotomy was created approximately 1 mm posterior to the limbus with a 30-gauge needle while carefully avoiding lens damage. A 35-gauge needle (NanoFil; World Precision Instruments, Inc., Sarasota, FL, USA) connected to a syringe (NanoFil; World Precision Instruments, Inc.) filled with 10 mg/mL sodium hyaluronate (Healon; Pharmacia and Upjohn Co., Kalamazoo, MI, USA) was introduced through the sclerotomy into the vitreous cavity. The tip was introduced into the subretinal space through a peripheral retinotomy, and 1 to 2 μL sodium hyaluronate was slowly injected until approximately one third of the retina became separated from the RPE.

Quantitative Real-Time PCR Analysis of Retinal mRNA Levels

Retinas were removed, flash-frozen in liquid nitrogen, and stored at −80°C until analysis. Total RNA was purified from retinal tissues using a column-based RNA purification kit (RNeasy Plus Mini kit; Qiagen Sciences, Germantown, MD, USA) with disposable tissue homogenizing devices (QiaShredders; Qiagen Sciences). Quantitative real-time polymerase chain reaction (qRT-PCR) was performed by reverse transcription of 0.8 to 1.0 μg of total RNA using random hexamers and oligo-dT primers in the presence of RNase inhibitor (Omni-

Investigative Ophthalmology & Visual Science

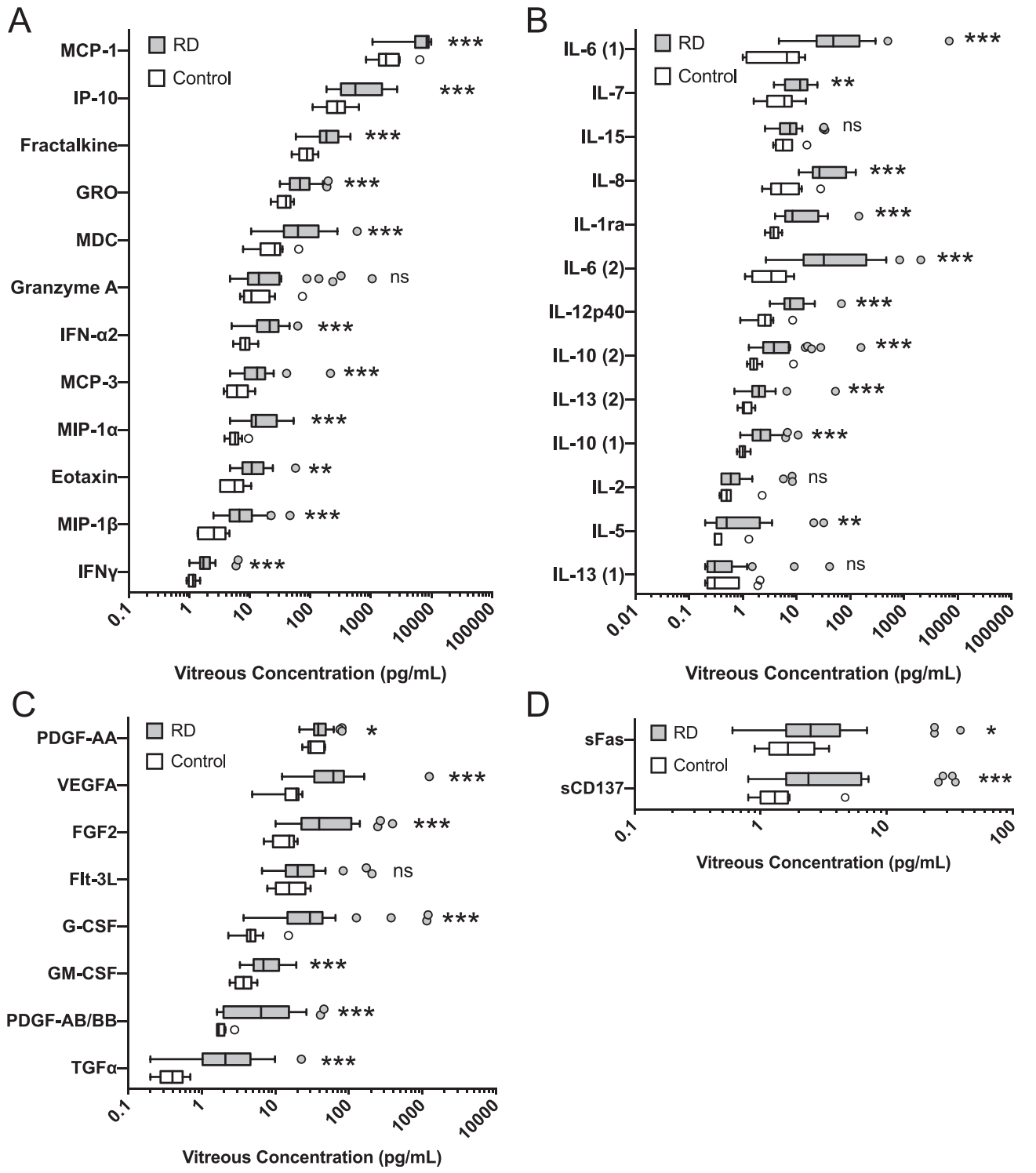

Figure 1. Effect of retinal detachment on human vitreous protein concentrations. Tukey box and whiskers plots with symbols showing outlying points for vitreous analyte concentrations from RD and control groups of patients, for (**A**) non-interleukin cytokines, (**B**) interleukin cytokines, (**C**) growth factors, and (**D**) soluble receptors. Analyte concentration values were obtained using two multiplex bead analyte panels as described in Methods. Repeated analytes represent concentrations obtained from panel 1 and panel 2. Significance of differences between groups were calculated using model-based fits of log normal distributions obtained from maximum likelihood estimation and are shown as $^{*}P \leq 0.05$, $^{**}P < 0.01$, and $^{***}P \leq 0.001$.

script RT kit; Qiagen). Duplex qRT-PCR was performed with gene-specific primers and FAM-labeled probes (Applied Biosystems Life Technologies, Foster City, CA, USA), along with β-actin–specific primers and VIC-labeled probes (primer limited formulation; Applied Biosystems Life Technologies) and universal PCR master mix (TaqMan; Applied Biosystems Life Technologies). Primer-probe assay information is provided in Supplementary Table S5. Reactions were performed and

fluorescence monitored using a CFX384 RT-PCR system (BioRad, Hercules, CA, USA). Relative normalized mRNA levels were calculated using the $\Delta\Delta C_t$ method. Statistical differences between like-treated sham and RD retina groups ($n = 3$ for sham control and $n = 4$ for RD group) were analyzed by Student's *t*-test.

Flow Cytometry of Retinal Cells

Following euthanasia, eyes were removed, retinas were quickly dissected, and RD or sham retinas pooled (two retinas per group) for processing as previous described.[31] Dissociated cells were resuspended in 50 µL of blocking buffer, PBS containing 20% rat serum and 1 µg/mL Mouse Fc-Block (rat anti-mouse CD16/CD32, clone 2.4G2; BD Biosciences, San Jose, CA, USA) and incubated for 20 minutes on ice. PerCP-Cy5.5-conjugated rat anti-mouse CD11b monoclonal antibody (1:100 dilution, clone M1/70; BD Bioscience), APC-Cy7-conjugated rat anti-mouse CD45 monoclonal antibody (1:100 dilution, clone 30-F11; BD Bioscience), PE-conjugated rat anti-mouse Ly6C monoclonal antibody (1:100 dilution, clone, HK1.4, eBioscience, San Diego, CA, USA), and FITC-conjugated anti-mouse Ly6G (Gr-1) monoclonal antibody (1:75 dilutions, clone RB6-8C5; eBioscience) were added and incubated for 45 minutes on ice. After rinsing three times in cold PBS, the cells were fixed in 1% paraformaldehyde for 30 minutes and analyzed using a flow cytometer (LSRII; BD Biosciences). An anti-mouse Ig microparticle compensation set (CompBeads; BD Biosciences) was incubated with each antibody pair for compensation corrections for spectral overlaps. Cytometer data were analyzed using software (FlowJo; Tree Star, Inc., Ashland, OR, USA). To exclude events representing debris and clumps of cells, events were gated in plots of forward scatter area (FSC-A) and side scatter area (SSC-A) and then gated in plots of forward scatter width (FSC-W) versus FSC-A in identical fashion for each group prior to analysis of CD11b, CD45, Ly6C, and Ly6G immunofluorescence intensities. $CD11b^{+}/CD45^{low}$ microglia were differentiated from $CD11b^{+}/CD45^{hi}$ myeloid leukocytes on the basis of their low expression of CD45.[32] Microglia were further defined as $CD11b^{+}/CD45^{low}/Ly6C^{neg}/Ly6G^{neg}$ cells. Myeloid leukocytes were subdivided into $CD11b^{+}/CD45^{hi}/Ly6C^{hi}/Ly6G^{neg}$ (inflammatory monocytes), $CD11b^{+}/CD45^{hi}/Ly6C^{neg}/Ly6G^{neg}$ (reparative monocytes), and $CD11b^{+}/CD45^{hi}/Ly6C^{low}/Ly6G^{neg}$ (intermediary monocytes), and $CD11b^{+}/CD45^{hi}/Ly6C^{neg}/Ly6G^{+}$ granulocytes. $CD11b^{neg}/CD45^{hi}$ cells representing lymphocytes were not further characterized. Statistical differences between like-treated sham and RD retina groups ($n = 4$ pooled samples/group at day 3) were analyzed by unpaired Student's *t*-test.

Immunofluorescence of Retinal Sections and Flat-Mounted Retinas

For immunofluorescence (IF) of retinal sections, mouse eyes were enucleated and fixed in 4% paraformaldehyde in PBS at 4°C overnight. After removing the anterior segments, the posterior eyecups were sequentially impregnated with a gradient concentration of sucrose in PBS for cryoprotection: 5% at room temperature (RT) for 1 hour, 10% at RT for 1 hour, and 20% at 4°C overnight. The eyecups were then embedded with a 1:1 mixture of 20% sucrose and optimal cutting temperature compound (Tissue-Tek 4583; Sakura Finetek, Torrance, CA, USA) and cut into 30-µm thick sections. The sections were air-dried and blocked with blocking buffer containing 10% goat serum in PBS with 0.3% Triton X-100 (PBST) at RT for an hour. The sections were then incubated with a mixture of primary antibodies diluted with blocking buffer at 4°C overnight. After three washes with PBST for 10 minutes each, the sections were incubated with a mixture of secondary antibodies and Hoechst-33342 at RT for an hour. The slides were rinsed with PBST three times for 10 minutes and mounted with mounting media (Prolong Gold; Thermo Fisher Scientific, Waltham, MA, USA). Images were captured with a confocal microscope (SP5; Leica Microsystems, Inc., Buffalo Grove, IL, USA) with a fixed detection gain for each comparative section.

For retinal flat mounting, mouse eyes were enucleated and punctured by an incision made through the corneas, followed by fixation in 4% paraformaldehyde in PBS at 4°C overnight. After several rinses with PBS, the anterior segments were dissected out under a dissecting microscope to create posterior eyecups. Retinas were carefully detached from the eyecup by positioning forceps between the retina and the underlying layers. After three washes in PBST, retinas were blocked with blocking buffer containing 10% goat serum in PBST at RT for 2 hours, followed by incubation with a mixture of primary antibodies including the following: rabbit polyclonal to the ionized calcium-binding adapter molecule 1 (Iba-1) (1:250, Cat. no. 019-19741; FUJIFILM Wako Chemicals USA Corp., Richmond, VA, USA) and rat monoclonal anti-Ki67 (1:100; Cat. no. 14-5698-82; eBioscience) in blocking buffer at 4°C for 42 to 46 hours. Retinas were then washed with PBST three times for 10 minutes, and incubated with a mixture of secondary antibodies including Alexa Fluor 488-conjugated goat anti-rabbit (1:1000, Cat. no. A-11034; Thermo Fisher Scientific) and Alexa Fluor 555-conjugated goat anti-rat (1:1000, Cat. no. A-21434; Thermo Fisher Scientific) with Hoechst-33342 (1:1000; Thermo Fisher Scientific) in blocking buffer at 4°C overnight. After three washes with PBST, four radial incisions were made from the edge of the eyecup halfway to the optic disc, and retinas were flat-mounted on 3-aminopropyltriethoxysaline-coated slides with Prolong Gold mounting media (Thermo Fisher Scientific). Images were captured with a confocal microscope (SP5; Leica Microsystems) with a fixed detection gain for each comparative section. For negative controls, the primary antibody was replaced with normal IgG (1 mg/mL) to examine the specificity and background IF.

Results

Characteristics of the Patient Population

A total of 24 RD patients and 10 controls were included in the study. The characteristics of these patients are shown in Table 1. The control group included three female patients with vitreous opacities and seven male patients, four with vitreous opacities and three with epiretinal membranes. For the RD cases, the extent of detachment ranged from 4 to 12 clock hours, with a mean of 7.52 (SD = 2.53). The duration from onset of symptoms to surgical repair ranged from 1 to 212 days, with a mean of 20.2 days (SD = 42.7 days). The mean initial BCVA for RD cases was logMAR = 1.44 (SD = 0.93). The initial BCVAs for patients who could read letters ranged from 20/30 (logMAR = 0.18) to 20/800 (logMAR =1.6), while four patients who could at best count fingers were assigned a logMAR = 2, and three patients who could see only hand motions were assigned a logMAR = 3.[33] Two additional patients were initially unable to see hand motions. The mean BCVA at follow-up was logMAR = 0.52 (SD = 0.58). For patients who could read letters at the final postoperative follow-up examination, BCVAs ranged from 20/20 (logMAR = 0) to 20/1250 (logMAR = 1.8), with one additional patient who could at best count fingers. The average improvement was 0.94 (SD = 0.70) on the logMAR scale.

Investigative Ophthalmology & Visual Science

Table 1. Patient Demographics

Group	RD	Control
Total number	24	10
Mean age (±SD)	61.8 (±13.3)	60.7 (±7.8)
Sex		
Female	6, 25%	3, 30%
Male	18, 75%	7, 70%
Indication	RRD with macular involvement, 100%	Vitreous opacities, 70% Epiretinal membrane, 30%

Effect of RD on Analyte Concentrations in Human Vitreous

Concentrations of 32 analytes were successfully compared in RD and control vitreous, and 28 of these were significantly increased in RD vitreous relative to control ($P \leq 0.05$). Summaries of observed and model-based vitreous analyte concentrations can be found in Supplementary Tables S3 and S4, respectively. Of the 12 non-interleukin cytokines compared, 11 were significantly increased in RD vitreous relative to control vitreous (Fig. 1A), including the following: eotaxin (2.4-fold, $P = 0.002$), fractalkine (2.4-fold, $P < 0.001$), GRO (2.1-fold, $P < 0.001$), IFN-α2 (2.7-fold, $P < 0.001$), IFNγ (1.9-fold, $P < 0.001$), IP-10 (3.1-fold, $P < 0.001$), MCP-1 (3.1-fold, $P < 0.001$), MCP-3 (3.2-fold, $P < 0.001$), MDC (4.2-fold, $P < 0.001$), MIP-1α (3.2-fold, $P < 0.001$), and MIP-1β (3.6-fold, $P < 0.001$). Granzyme A exhibited no significant difference in vitreous concentrations between groups. MCP-1 exhibited by far the highest mean concentrations of any analyte tested, at 2.3 μg/mL in control vitreous and 7.2 μg/mL in RD vitreous.

A total of 10 cytokines designated as interleukins were successfully compared, and seven of these were increased in RD versus control vitreous (Fig. 1B). These include IL-1RA (5.0-fold, $P < 0.001$), IL-5 (7.4-fold, $P = 004$), IL-6 (first panel, 58-fold, $P < 0.001$; second panel, 48-fold, $P < 0.001$), IL-7 (1.9-fold, $P = 0.003$), IL-8 (5.8-fold, $P < 0.001$), IL-10 (first panel, 2.9-fold, $P < 0.001$; second panel, 5.5-fold, $P < 0.001$), and IL-12p40 (3.9-fold, $P < 0.001$). The two multiplex panels produced contradictory results for IL-13 (first panel, 3.7-fold, $P < 0.001$; second panel, 3.9-fold, $P = 0.82$). IL-15 exhibited the highest mean concentration in control vitreous (6.7 pg/mL) of any interleukin, which was not significantly affected by RD. In RD vitreous IL-6 exhibited the highest mean concentration (first panel, 381 pg/mL; second panel, 198 pg/mL), followed by IL-8 (47 pg/mL).

Seven of the eight successfully tested growth factors were significantly increased in RD vitreous versus control vitreous (Fig. 1C), including: FGF2 (5.6-fold, $P < 0.001$), G-CSF (26-fold, $P < 0.001$), GM-CSF (2.1-fold, $P < 0.001$), PDGF-AA (1.3-fold, $P = 0.042$), PDGF-AB/BB (5.8-fold, $P < 0.001$), TGF-α (8.8-fold, $P < 0.001$), and VEGFA (6.7-fold, $P < 0.001$). Flt-3L was not significantly increased in RD vitreous. Whereas PDGF-AA exhibited the highest mean concentration in control vitreous at 34 pg/mL, G-CSF exhibited the highest mean concentration in RD vitreous at 145 pg/mL.

The two soluble receptors tested both exhibited significantly increased concentration in RD versus control vitreous (Fig. 1D): sCD137 (4.7-fold, $P = 0.001$) and sFas (3.0-fold, $P = 0.045$). These proteins exhibited relatively low concentrations, with means of only 7.7 pg/mL and 5.8 pg/mL in the RD vitreous samples, respectively.

Associations Between Clinical Covariates With Vitreous Analyte Concentrations

Regression analysis was used to compare analyte concentrations with the characteristics of the subject populations, including duration of detachment, extents of detachment, pre- and postoperative BCVAs, and changes in BCVA (Table 2). None of the analytes were significantly influenced by age. It is interesting that the vitreous concentration of only one analyte, PDGF-AA, exhibited a significant association with sex (combined RD and control subjects), with a higher mean vitreous PDGF-AA concentration in females (1.3-fold, $P = 0.035$). Vitreous concentrations of 31 analytes exhibited positive association (positive β coefficients) with the extent of detachment in RD cases. The vitreous concentrations of six analytes, sCD37, EGF, Flt3L, IL-2, IL-10, and PDGF-AA, were positively associated with duration of detachment. Vitreous concentrations of 12 analytes exhibited positive associations with the preoperative BCVA logMAR values, indicating a tendency for lower VA in patients with higher vitreous concentrations. Concentrations of 27 analytes positively associated with the postoperative BCVA logMAR values obtained at the last follow-up exam, again indicating a tendency for worse VA in patients with higher vitreous concentrations. None of the analytes exhibited a negative association (negative β coefficients) with pre- or postoperative logMAR values. Vitreous concentrations of 11 analytes positively associated with both pre- and postoperative logMAR values. Interestingly, none of the analyte concentrations significantly associated with the change in logMAR values from pre- to postoperative exams.

Effect of RD on Mouse Retinal Inflammatory Gene Expression

We used a mouse model of RD to examine the effect of RD on expression of selected numbers of mRNAs corresponding to analytes increased in human vitreous. The rodent model results in approximately one third of the neural retina to be continuously detached from the RPE, corresponding to approximately 4 clock hours of detachment in humans. Detached and contralateral control retinas undergoing only a scleral needle puncture were harvested 7 days after detachment, and qRT-PCR was used to examine relative mRNA levels (Fig. 2 and Supplemental Table S3). Levels of mRNAs corresponding to the chemokines CCL2 (encoding MCP-1), CCL3 (MIP-1α), and CXCL10 (IP-10), as well as Fas, were all increased by more than 1000-fold in RD relative to control retinas. Expression of CX3CL1 (fractalkine) mRNA was upregulated by nearly 14-fold. TNFA (TNFα) mRNA was increased by approximately nine-fold in RD retinas. CCL22 (MDC) mRNA trended toward a 70% reduction while IL-15 mRNA was decreased by 25%. In contrast to human vitreous results, of the three growth factor mRNAs tested in mice, FLT3L, PDGFA, and VEGFA, only FLT3L mRNA was increased (4.5-fold) in mouse RD retinas. We also failed to detect CXCL1 (GRO), IFNA2, IL-6, IL-7, and FGF2 mRNA in the mouse retina (data not shown). Thus, the mouse RD model exhibited marked inflammatory response with increases in expression of mRNA for a number of cytokines that were increased in human RD vitreous but did not mimic the growth factor upregulation evidenced in humans.

Effect of RD on Murine Retinal Innate Immune Cell Populations

We used flow cytometry to examine microglial and leukocyte populations in the mouse retina at 1 and 3 days following experimental RD (Fig. 3A). Immune cell populations were first defined by gating on the common leukocyte marker CD45, and the myeloid lineage marker CD11b and microglia and myeloid leukocytes were further defined by gating for Ly6C, a marker of inflammatory monocytes, and the granulocyte/neutrophil

Table 2. Correlations Between Analytes and Covariates

Analyte	Extent of Detachment, β, *P* Value	Duration of Detachment, β, *P* Value	Initial BCVA, β, *P* Value	Final BCVA, β, *P* Value	Change in BCVA, β, *P* Value
Cytokines					
sCD40L	**0.19, 0.001**	0.34, 0.24	0.18, 0.267	0.53, 0.063	−0.03, 0.91
Eotaxin	**0.09, 0.03**	0.31, 0.11	0.16, 0.117	**0.51, 0.003**	0.04, 0.80
Fractalkine	**0.08, 0.04**	0.16, 0.37	0.17, 0.115	**0.46, 0.002**	0.02, 0.91
Granzyme A	**0.27, 0.004**	0.81, 0.08	**0.48, 0.050**	**1.4, 0.000**	0.07, 0.86
Granzyme B	**0.30, 0.01**	0.01, 0.98	**0.68, 0.02**	**0.92, 0.04**	−0.82, 0.13
GRO	**0.10, 0.002**	0.02, 0.90	0.02, 0.87	0.20, 0.22	0.14, 0.40
IFNα2	**0.10, 0.04**	0.06, 0.78	0.06, 0.68	0.33, 0.12	0.14, 0.52
IFNγ (1)	**0.11, 0.000**	0.09, 0.57	0.08, 0.33	0.25, 0.08	−0.01, 0.96
IFNγ (2)	0.26, 0.09	0.65, 0.36	0.22, 0.54	0.69, 0.322	−0.10, 0.85
IP-10	**0.20, 0.001**	0.43, 0.16	0.31, 0.10	**1.1, 0.000**	0.25, 0.39
MCP-1	0.04, 0.31	−0.16, 0.38	0.12, 0.34	0.22, 0.21	−0.06, 0.76
MCP-3	**0.16, 0.003**	0.42, 0.10	**0.24, 0.03**	**0.61, 0.009**	−0.09, 0.62
MDC	**0.17, 0.015**	0.53, 0.11	0.29, 0.19	**0.86, 0.003**	0.15, 0.64
MIP-1α (1)	**0.16, 0.000**	0.21, 0.34	0.21, 0.12	**0.58, 0.002**	0.04, 0.85
MIP-1α (2)	**1.13, 0.000**	0.42, 0.80	0.09, 0.93	1.5, 0.30	1.21, 0.46
MIP-1β (1)	**0.16, 0.000**	0.20, 0.40	0.10, 0.42	0.29, 0.19	−0.04, 0.82
MIP-1β (2)	**0.15, 0.03**	0.22, 0.50	0.12, 0.53	0.23, 0.46	−0.14, 0.59
Interleukins					
IL-1ra	**0.14, 0.03**	0.56, 0.053	0.17, 0.30	**0.61, 0.03**	0.07, 0.78
IL-2	**0.17, 0.02**	**0.75, 0.02**	**0.42, 0.03**	**0.86, 0.003**	−0.15, 0.69
IL-4	**0.13, 0.004**	0.14, 0.55	0.17, 0.16	**0.46, 0.03**	−0.02, 0.91
IL-5	**0.30, 0.001**	0.49, 0.28	**0.50, 0.03**	**0.94, 0.03**	−0.38, 0.31
IL-6 (1)	**0.32, 0.003**	−0.04, 0.94	0.22, 0.54	0.83, 0.10	0.27, 0.62
IL-6 (2)	**0.35, 0.003**	−0.18, 0.76	0.31, 0.42	0.93, 0.09	0.14, 0.80
IL-7	0.07, 0.09	0.13, 0.51	**0.23, 0.050**	**0.51, 0.002**	−0.06, 0.76
IL-8	**0.21, 0.000**	0.23, 0.40	0.16, 0.362	**0.52, 0.04**	0.08, 0.75
IL-10 (1)	**0.14, 0.000**	0.22, 0.32	**0.27, 0.02**	**0.67, 0.000**	−0.05, 0.81
IL-10 (2)	**0.19, 0.015**	**0.92, 0.006**	**0.40, 0.01**	**1.00, 0.001**	−0.11, 0.68
IL-12p40	**0.16, 0.001**	0.33, 0.16	**0.27, 0.02**	**0.58, 0.006**	−0.14, 0.46
IL-12p70	**0.17, 0.000**	0.32, 0.16	0.17, 0.18	**0.52, 0.015**	0.02, 0.92
IL-13 (1)	**0.15, 0.009**	0.44, 0.11	0.12, 0.26	0.41, 0.13	−0.04, 0.80
IL-13 (2)	**0.40, 0.001**	0.81, 0.15	0.44, 0.11	1.0, 0.06	−0.25, 0.55
IL-15	0.08, 0.14	0.39, 0.11	**0.33, 0.02**	**0.76, 0.000**	−0.08, 0.73
Growth factors					
EGF	**0.20, 0.001**	**0.66, 0.02**	0.10, 0.38	0.50, 0.07	0.11, 0.55
FGF2	**0.17, 0.02**	0.49, 0.15	**0.38, 0.049**	0.63, 0.051	−0.34, 0.26
Flt-3L	0.13, 0.06	**0.63, 0.02**	**0.37, 0.04**	**1.0, 0.000**	0.73, 0.80
G-CSF	**0.35, 0.000**	0.74, 0.14	0.52, 0.12	**1.5, 0.000**	0.29, 0.58
GM-CSF	**0.11, 0.000**	0.14, 0.38	0.10, 0.29	**0.32, 0.03**	0.03, 0.81
PDGF-AA	0.03, 0.21	**0.23, 0.04**	0.13, 0.06	**0.30, 0.003**	−0.03, 0.78
PDGF-AA/BB	0.13, 0.20	0.58, 0.18	0.48, 0.08	**1.1, 0.004**	−0.09, 0.83
TGFα	0.10, 0.26	−0.06, 0.87	0.12, 0.65	**0.41, 0.26**	0.07, 0.86
VEGF	**0.16, 0.009**	0.52, 0.07	0.23, 0.07	**0.69, 0.010**	−0.02, 0.93
Soluble receptors					
sCD137	**0.22, 0.007**	**0.96, 0.01**	0.45, 0.06	**1.1, 0.001**	0.13, 0.77
sFas	**0.17, 0.03**	0.67, 0.06	**0.46, 0.02**	**1.2, 0.000**	0.002, 1.00

Extent of detachment in clock values. Duration of attachment in log10(days). BVCA in logMAR. For repeated analytes, numbers in parentheses indicate multiplex panel number (see Methods). Significant correlations ($P \leq 0.05$) are shown in bold type.

marker Ly6G. No increases in microglia, myeloid leukocyte, or lymphocyte numbers were found at 1 day, whereas all three populations were significantly increased at 3 days after detachment. Microglia were increased by 1.9-fold, myeloid leukocytes were increased by 2.1-fold, and lymphocytes were increased by 1.7-fold. Subdivision of myeloid leukocytes revealed that $Ly6C^{neg}$ reparative monocytes numbers were significantly increased by 1.9-fold, and $Ly6C^{hi}$ inflammatory monocytes were increased by 4.8-fold. Granulocytes numbers were vanishingly small in control retinas, but increased by 10-fold at 3 days after RD. Thus, the inflammatory response to RD in the mouse included an increase in microglia, inflammatory monocytes, reparative monocytes, granulocytes, and lymphocytes.

In order to test if the increase in the microglial numbers following RD involved expansion of the resident retinal microglia population, expression of the proliferation marker Ki67 was examined. Immunofluorescence of flat-mounted control and RD retinas at 2 and 3 days following RD revealed cells with ramified morphologies resembling microglia that were positive for both Ki67 and Iba-1 only in RD retinas (Fig. 3B). These costained cells were most prevalent at 2 days after

Investigative Ophthalmology & Visual Science

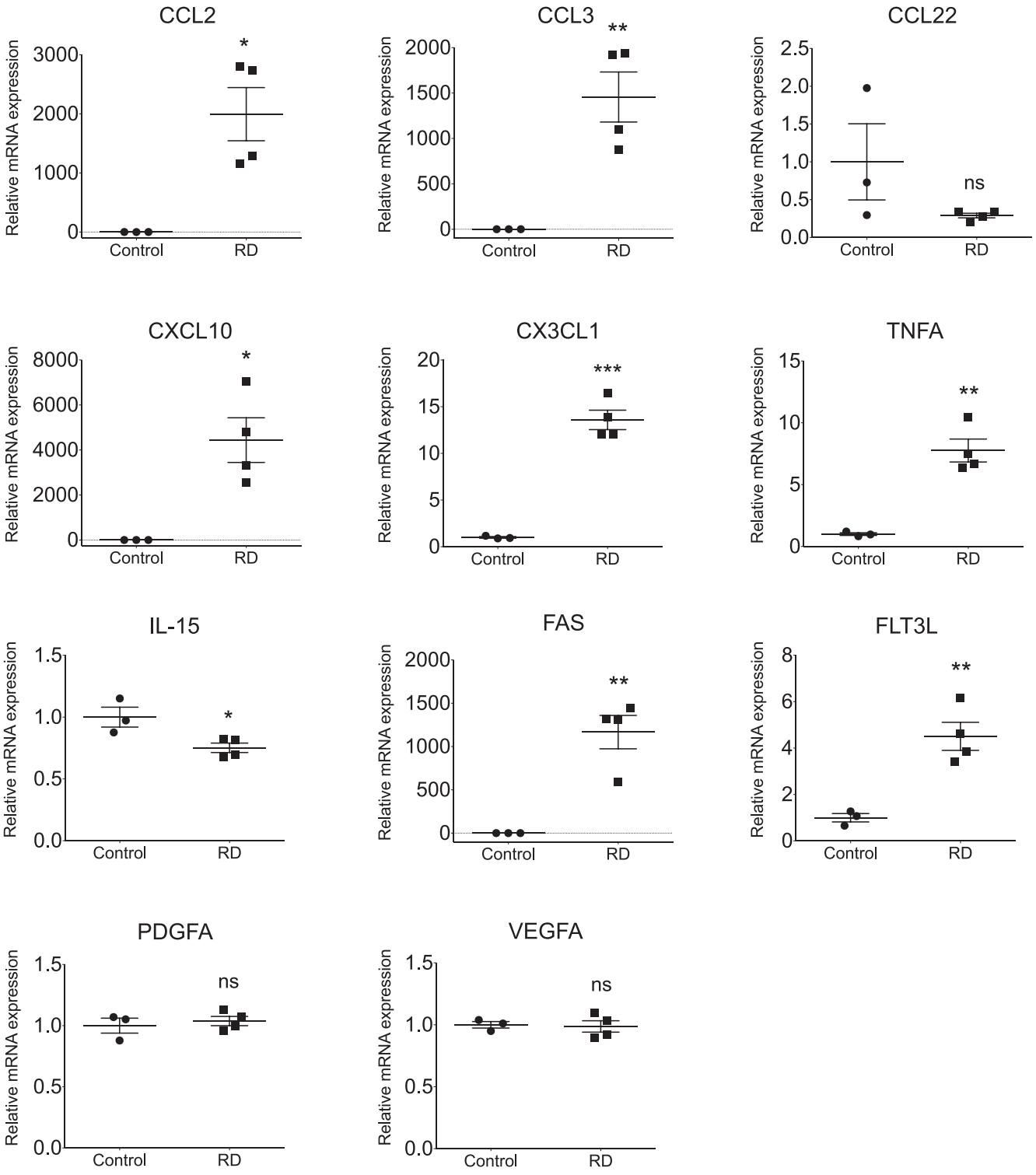

Figure 2. Effect of RD on mouse retinal gene expression. Levels of mRNAs in mouse retinas with detachments and scleral puncture controls at 7 days after detachment were measured by duplex qRT-PCR with normalization to β-actin mRNA. Relative mRNA values are normalized to the mean of control values. Mean and standard errors are shown, along with individual symbols representing actual data values ($n = 3$ for control, $n = 4$ for RD). Significance of differences between groups were calculated using Student's t-test and are shown as $^{*}P \leq 0.05$, $^{**}P \leq 0.01$, and $^{***}P \leq 0.001$.

RD. In addition, Ki67 staining revealed numerous microglial forms that appeared to be binucleated, further suggesting that these were either in the process of cell division or were daughter cells resulting from cellular division. This analysis also revealed a marked difference in morphology of Iba-1^{+} presumptive microglia, with a pronounced shortening and thickening of cellular processes and increase in soma size.

Retinal detachment causes a pronounced stress to PR cells, resulting in their eventual death.[34] To determine if microglia migrated toward stressed PR following RD, Iba-1 immuno-

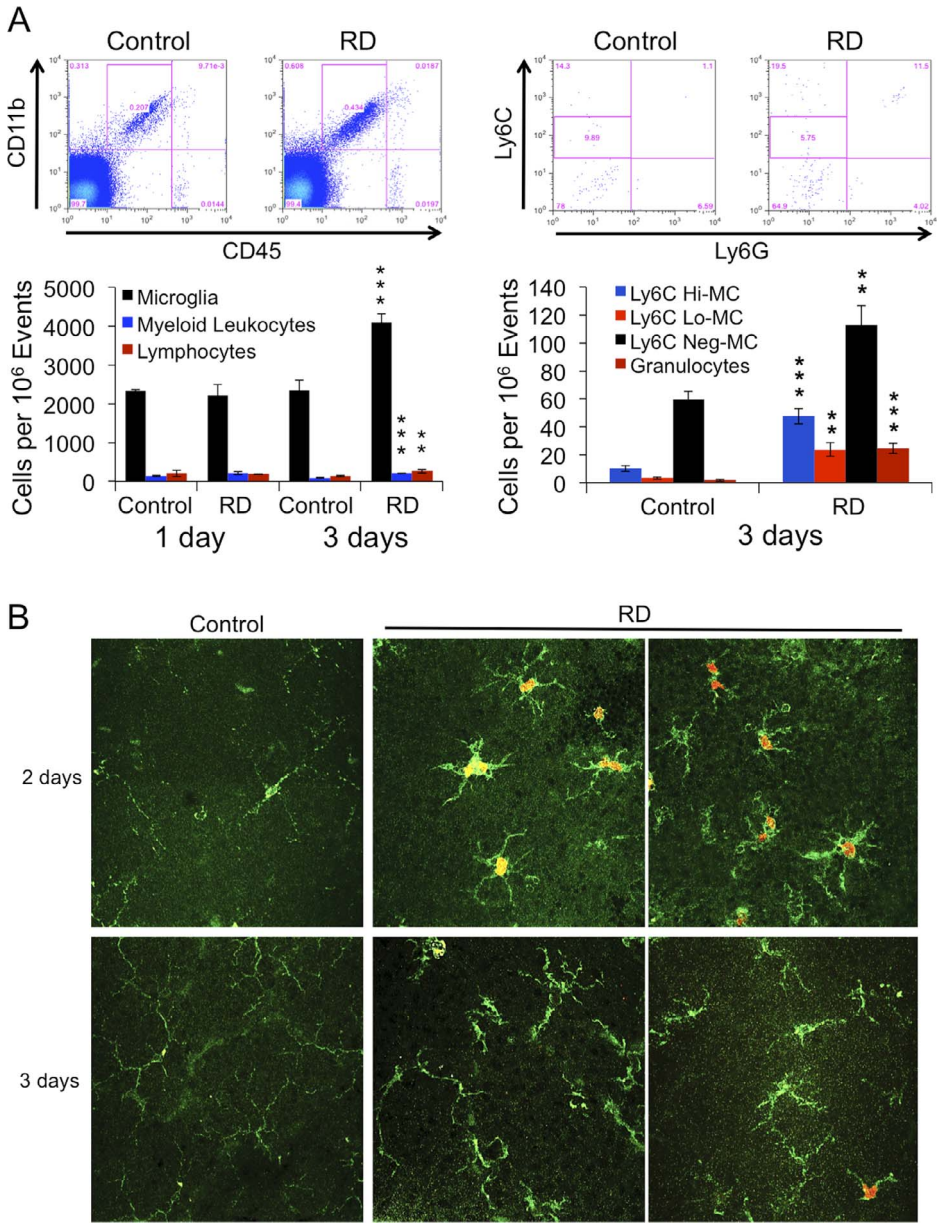

Figure 3. Effect of RD on mouse retinal microglia and leukocyte populations. (**A**) Flow cytometry of microglia and leukocyte populations in the mouse retina at 1 day ($n = 2$/group) and 3 days ($n = 4$/ group) following experimental RD. Populations were defined by gating on the leukocyte common antigen CD45 and the myeloid lineage marker CD11b. Gating for inflammatory monocyte marker Ly6C and granulocyte/neutrophil marker Ly6G further defined populations of microglia and subpopulations of myeloid leukocytes. (**B**) Immunofluorescence of flat-mounted mouse retinas at 2 and 3 days after detachment showing the proliferation of microglia. Iba-1$^+$ (*green*) cells with ramified morphology are microglia; Ki67 (*red*) is a proliferative cell marker.

fluorescence was examined in retinal sections at 1, 2, 3, and 7 days after RD (Fig. 4A). Relatively thick (30 µm) vertical sections were used to encompass a considerable fraction of horizontally oriented microglia dendritic process arbors, which span approximately 70 µm in the mouse retina.[35] The analysis demonstrated a spatial disruption of microglia and their apparent movement toward the outer nuclear layer (ONL) and subretinal space after 3 and 7 days. Iba-1$^+$ cells with a round morphology were also observed in the subretinal space at 3 and 7 days, which may represent amoeboid microglia or Iba-1$^+$ invading monocytes. To confirm the migration of microglia, RD and contralateral control retinas were flat-mounted at 3 days after detachment and probed with antibody to Iba-1 (Fig. 4B). Whereas control retinas contained virtually no Iba-1$^+$ cells in the ONL and at the level of PR inner segments (IS) and outer segments (OS), RD retinas contained numerous Iba-1$^+$ cells with moderately ramified morphologies indicative of microglia in an intermediate state of activation. Thus, this analysis suggests that microglia react to RD by activating, proliferating, and mobilizing toward distressed PR.

Discussion

The present study highlights the innate immune response to RD in patients and a mouse RD model. The increase in vitreous cytokine concentrations in human RD, the increase in cytokine mRNA expression, attraction of leukocytes, and microglial

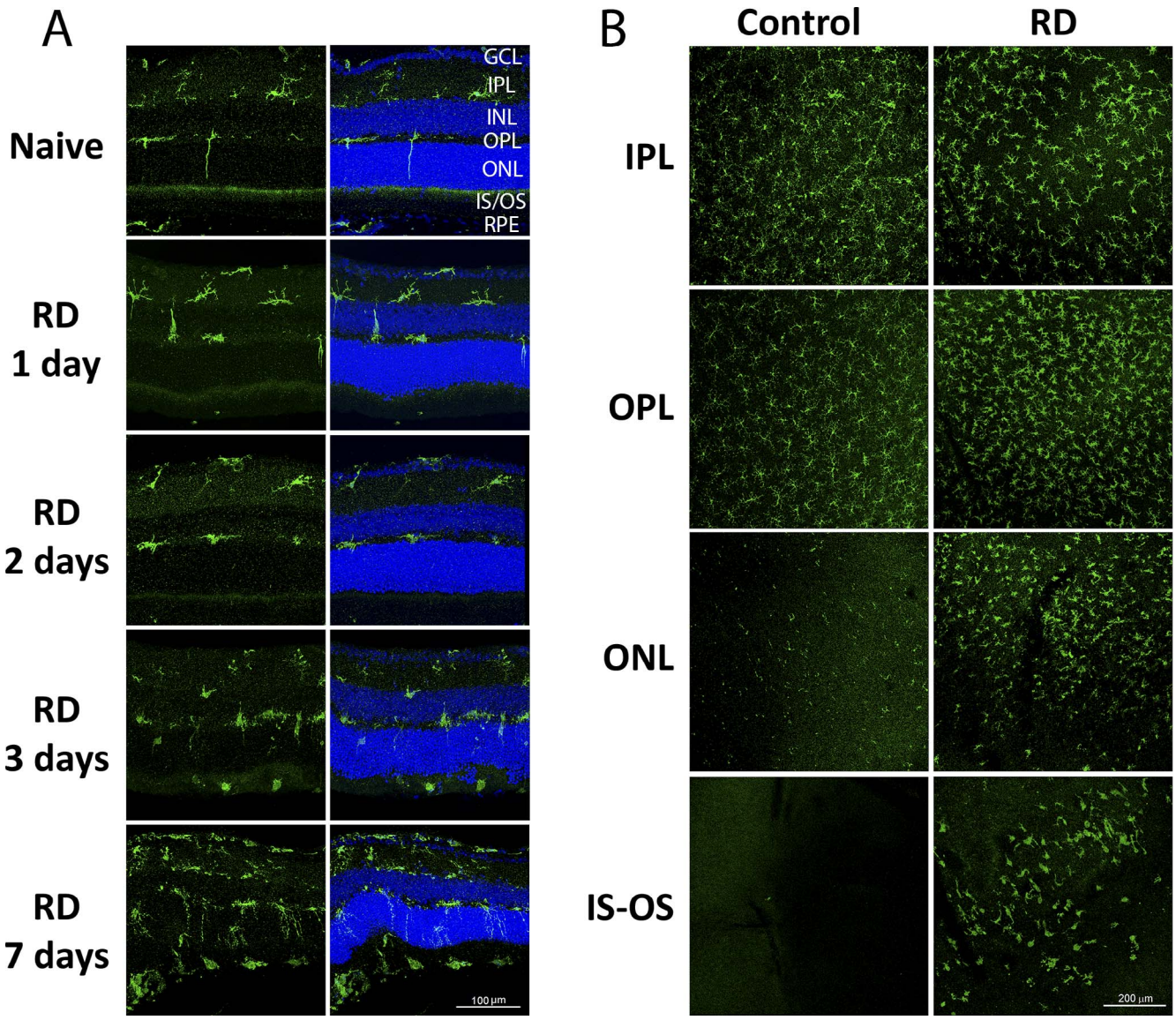

FIGURE 4. Effect of RD on retinal microglia location and morphology. Vertical retinal sections (**A**) and flat-mounted retinas (**B**) at 1, 2, 3, and 7 days after RD with Iba-1$^+$ immunofluorescence (*green*) showing the mobilization of microglia to the ONL following detachment. *Blue fluorescence* is DAPI staining of cell nuclei.

response in the mouse model all show that sterile inflammation is a significant component of the retina's response to separation from the RPE. In addition, concentrations of several growth factors were largely increased in vitreous from RD patients relative to controls. This general growth factor upregulation was apparently not recapitulated in the mouse model at the time examined.

Analysis of concentrations of 32 analytes, including cytokines, growth factors, and soluble receptors in vitreous from RD patients and controls, demonstrated that 28 factors were significantly increased following RD. Failed comparisons were mainly due to an excess of samples below the lower limit of detection in the control vitreous samples, suggesting that a significant increase in RD vitreous might be reliably identified for additional analytes if higher sensitivity assays were employed. Of particular relevance are the cytokines MCP-1, IP-10, fractalkine, GRO, MDC, IL-6, and IL-8, all of which exhibited relatively high concentrations and several-fold increases in the vitreous of RD patients. In addition, seven growth factors and two soluble receptors exhibited significantly elevated concentrations in RD vitreous. Although some analytes were unchanged by RD, none were decreased. Kunikata and coworkers[12] examined 17 analytes in the aqueous humor of RRD patients, representing a subset of the analytes tested in the present study. These authors found significant increases in aqueous levels of eotaxin, G-CSF, IFNγ, IL-6, IL-8, IP-10, MCP-1, MIP-1β, TNFα, and VEGF, while FGF2, GM-CSF, MIP-1α, PDGF-AB/BB, and RANTES were not significantly increased. The wide-ranging increase in aqueous and vitreous cytokines suggests that there is a broad neuroinflammatory response to RD.

The present study found that the majority of cytokines (including interleukins) were positively correlated with the extent of detachment. Thus, the inflammatory response increases with the severity of the disorder. Takashi and coworkers[36] recently found that IL-6, IL-8, IP-10, MCP-1, and MIP-1β were all increased in RRD patient vitreous versus macular hole controls. However, these authors found that only IL-8 and MIP-1β were correlated with the extent of detachment. Similarly, Pollreisz and colleagues[7] recently found that IL-

Investigative Ophthalmology & Visual Science

6, IL-8, IP-10, MCP-1, and MIP-1α, were significantly increased in vitreous of RRD patients, but only IL-8 was significantly correlated with the extent of detachment. Given that IL-8 (CXCL8) is a potent granulocyte chemoattractant, these results suggest that neutrophils may play a role in the response to RD. In fact, in the mouse RD model we observed a significant increase in granulocyte numbers, which are likely to be almost entirely neutrophils.

It is interesting that although many cytokines were correlated with the extent of detachment, only two, IL-2 and IL-10, showed any association with the duration of detachment. Given that these two cytokines are relatively anti-inflammatory, this suggests that inflammation is not particularly progressive following RD. A recent paper demonstrated that IL-10 inhibited both VEGF expression and proliferation of cultured retinal pigmented epithelial cells isolated from rat eyes following RD.[37]

The present study raises the possibility that inflammation is a key driver of loss of vision following RD. Vitreous concentrations of several analytes were negatively associated with either preoperative BCVA or postoperative BCVA, as indicated by a positive β coefficient with logMAR values. Eleven analytes were negatively associated with both pre- and postoperative BCVA. These include nine cytokines and interleukins, as well as Flt-3L and sFas. Flt-3L may also be considered a cytokine for its role in dendritic cell development.[38] This finding suggests that inflammation may contribute to the temporary and permanent loss of vision in RD patients. However, no significant associations were observed between these analytes and the improvement in VA following surgical treatment (change from pre- to postoperative). It should be noted that there was also a positive association between the extent of detachment and the final BCVA ($P = 0.006$), and multiple regression analysis was not done to separate the relationships between variables. A larger study is required to isolate cause-and-effect relationships by multiple regression analysis. However, the fact that many of the analytes significantly associated with final BCVA are not significantly associated with extent of detachment argues that these are independent variables.

RD caused increased vitreous levels of seven of the eight growth factors tested. Of these, FGF2, G-CSF, PDGF-AB/BB, and VEGF levels were all previously reported as increased in vitreous or subretinal fluid of RD patients.[7,11,13,39–41] However, a previous study also found that FGF2 and PDGF levels were increased in vitreous of patients with PVR but not in vitreous of patients with RD and no PVR.[42] To the best of our knowledge the present study is the first to examine the effects of RD on vitreous EGF, Flt3l, G-CSF, GM-CSF, and TGFα levels. Of particular interest, the colony-stimulating factors, G-CSF and GM-CSF, were significantly increased in the RD vitreous versus controls and significantly correlated with the extent of detachment and postoperative VA. It should be noted that G-CSF and GM-CSF might be better characterized as cytokines, as they function as granulocyte, monocyte, and hematopoietic stem cell motility factors as well as growth factors.[43,44] G-CSF also has neuroprotective properties and inhibits photoreceptor degeneration in a mouse light-induced retinal damage model.[45,46]

The levels of soluble receptors tested, sFas and sCD137, were elevated in RD relative to control. sFas and Fas ligand (FasL) have been shown to be elevated in subretinal fluid of RD patients with higher levels in PVR versus non-PVR patients.[47] The interaction of the Fas receptor with membrane-bound FasL triggers Fas-mediated apoptosis. We have previously shown in a rodent model that Fas and FasL are upregulated and associated following RD.[48] Inhibition of Fas in a rat RD model decreased photoreceptor death.[48,49] Soluble Fas may act as a decoy to prevent photoreceptor apoptosis following detachment. CD137 is a member of the TNF receptor superfamily that is expressed upon activation of T lymphocytes. The soluble form sCD137 arises by differential splicing and is thought to decrease T lymphocyte activation and antigen presentation and to promote T-cell death.[50] In the eye, CD137 neutralizing antibody inhibited the induction of experimentally induced uveitis,[51] but to our knowledge no role in the setting of RD has been studied.

In the mouse RD model expression of mRNAs corresponding to MCP-1 (CCL2), MIP-1α (CCL3), IP-10 (CXCL10), fractalkine (CX3CL1), Fas, Flt3l, and TNFα (TNFA) were all markedly increased after 7 days of detachment. MRNAs corresponding to MDC (CCL22), PDGFA, and VEGFA were unchanged, and IL-15 mRNA was slightly decreased. Zeng and coworkers[52] found marked increases in expression of CCL2, CCL3, and CXCL10 cytokine mRNAs in the rd mouse model of retinal degeneration. In that model chemokine mRNA upregulation slightly preceded the appearance of $CD11b^+$ cells in the ONL, which in turn slightly preceded PR apoptosis. In a model of chronic light-induced PR degeneration, Natoli and colleagues[53] similarly observed increased CCL2, CCL3, and CCL12 (MCP-5) mRNA expression preceding the appearance of $Iba\text{-}1^+$ and $F4/80^+$ microglia/macrophages to the ONL and subretinal space. MCP-1, MIP-1α, MIP-1β, IP-10, and fractalkine all act as monocyte/macrophage chemoattractants capable of inducing microglial migration.[54,55] If expressed in the outer retina or the RPE, gradients of these chemokines could contribute to the attraction of resident microglia and infiltrating monocytes to distressed PR following RD.

To the best of our knowledge this is the first study to implicate fractalkine (CX3CL1) in the response to RD. CX3CL1 is a key regulator of microglial function and a microglial chemoattractant.[55] CX3CL1 is a transmembrane protein that is highly expressed by neurons. In response to stress, the ectodomain of CX3CL1 is shed to form soluble CX3CL1. Thus, the increased concentration of soluble fractalkine in vitreous of the RD patient may represent its proteolytic cleavage from PR rather than upregulation of expression. Increased CX3CL1 mRNA expression in the mouse retina suggests that its de novo expression may also be increased. In neural tissue, expression of the fractalkine receptor, CX3CR1, is restricted to microglia, and the CX3CL1-CX3CR1 pair are key regulators of neuron-microglia communication.

The greatly increased expression of chemokines, including fractalkine, suggests that RD may cause microgliosis and an attraction of leukocytes to the detached retina. An accumulation of bone marrow–derived cells, principally monocytes/macrophages, following detachment of mouse and rat retinas has been qualitatively documented by several authors.[17,19,25,56–59] In addition, lectin staining and CD11b immunofluorescence of retinal sections suggested an increase in microglial numbers after RD in the cat, ground squirrel, and human.[22] Using established flow cytometry methods[32,60–62] we were able to characterize the microglia and leukocyte populations attracted to the detached retina and to show that microglia, $Ly6C^{hi}$ inflammatory monocytes, $Ly6C^{neg}$ reparative monocytes, granulocytes (presumably neutrophils), and lymphocytes were all significantly increased following RD. Microglial numbers doubled from day 2 to day 3 after RD. Ki67 expression and binucleation of $Iba\text{-}1^+$ cells resembling microglia were also observed at 2 days after RD. These presumptive microglia also presented a less ramified morphology, mobilized from the plexiform layers and migrated toward the ONL and subretinal space during this time. $Iba\text{-}1^+$ cells with amoeboid morphologies appeared in the subretinal space and may represent fully activated microglia or Iba-1 expressing monocyte-derived macrophages. Attraction of microglia/mono-

cytes to the outer retina following detachment has been well documented. An early study using lectin staining and CD11b immunofluorescence of retinal sections suggested that retinal microglial numbers were increased after RD in the cat, ground squirrel, and human.[22] Two recent studies identified $CD11b^+$ cells in the subretinal space of mice as soon as 12 hours after RD.[17,56] Recently, Wang and coworkers[59] used flow cytometry of CD11b and isolectin B4 to show increases in monocytes after only 1 day of RD in the mouse. Two previous studies showed an increase in $CD11b^+$ bone marrow–derived cells at 3 days after RD in the mouse.[19,57] However, myeloid cell markers, including CD11b and Iba-1, cannot fully distinguish between microglia and macrophages.[63] Thus, the precise identities of cells observed in the subretinal space following RD are still unclear.

Although an inflammatory response to RD seems certain, there is an apparent need to determine if this inflammatory response contributes to an irreversible loss of VA and if anti-inflammatory treatments can preserve vision in RD patients. Toward this goal, the mouse RD model could prove useful to determine the role of microglia activation and invading leukocytes in PR death and survival following RD.

Acknowledgments

Supported by The Heed Foundation (LK); Michigan Ophthalmic Trainee Career Development Award (LK); Research to Prevent Blindness (LK); Sybil B. Harrington Physician Scientist Award from Research to Prevent Blindness (DNZ); Foundation Fighting Blindness (DNZ); National Eye Institute Grants R01-EY020823 (DNZ) and R01-EY020582 (SFA); and Grant P30-EY007003, University of Michigan Core Center for Vision Research.

Disclosure: **L. Kiang**, P; **B.X. Ross**, None; **J. Yao**, None; **S. Shanmugam**, None; **C.A. Andrews**, None; **S. Hansen**, None; **C.G. Besirli**, P; **D.N. Zacks**, ONL Therapeutics (C, I), P; **S.F. Abcouwer**, None

References

1. Kwon OW, Song JH, Roh MI. Retinal detachment and proliferative vitreoretinopathy. *Dev Ophthalmol*. 2016;55:154–162.
2. Wang S, Linsenmeier RA. Hyperoxia improves oxygen consumption in the detached feline retina. *Invest Ophthalmol Vis Sci*. 2007;48:1335–1341.
3. Shelby SJ, Angadi PS, Zheng QD, Yao J, Jia L, Zacks DN. Hypoxia inducible factor 1alpha contributes to regulation of autophagy in retinal detachment. *Exp Eye Res*. 2015;17:84–93.
4. Besirli CG, Chinskey ND, Zheng QD, Zacks DN. Autophagy activation in the injured photoreceptor inhibits Fas-mediated apoptosis. *Invest Ophthalmol Vis Sci*. 2011;52:4193–4199.
5. Mahmoudi S, Almony A. Macula-sparing rhegmatogenous retinal detachment: is emergent surgery necessary? *J Ophthalmic Vis Res*. 2016;11:100–107.
6. Lo AC, Woo TT, Wong RL, Wong D. Apoptosis and other cell death mechanisms after retinal detachment: implications for photoreceptor rescue. *Ophthalmologica*. 2011;226:10–17.
7. Pollreisz A, Sacu S, Eibenberger K, et al. Extent of detached retina and lens status influence intravitreal protein expression in rhegmatogenous retinal detachment. *Invest Ophthalmol Vis Sci*. 2015;56:5493–5502.
8. Yoshimura T, Sonoda KH, Sugahara M, et al. Comprehensive analysis of inflammatory immune mediators in vitreoretinal diseases. *PLoS One* 2009;4:e8158.
9. Symeonidis C, Androudi S, Georgalas I, et al. Chemokine CXCL-1: activity in the vitreous during proliferative vitreoretinopathy. *Clin Exp Immunol*. 2015;181:338–342.
10. Symeonidis C, Androudi S, Tsaousis KT, et al. Comparison of interleukin IL-6 levels in the subretinal fluid and the vitreous during rhegmatogenous retinal detachment. *Cytokine*. 2012;57:17–18.
11. Danielescu C, Zugun-Eloae F, Zlei M. Concentrations of vitreal cytokines in rhegmatogenous retinal detachment. *Rev Med Chir Soc Med Nat Iasi*. 2016;120:124–129.
12. Kunikata H, Yasuda M, Aizawa N, Tanaka Y, Abe T, Nakazawa T. Intraocular concentrations of cytokines and chemokines in rhegmatogenous retinal detachment and the effect of intravitreal triamcinolone acetonide. *Am J Ophthalmol*. 2013;155:1028–1037.e1.
13. Rasier R, Gormus U, Artunay O, Yuzbasioglu E, Oncel M, Bahcecioglu H. Vitreous levels of VEGF, IL-8, and TNF-alpha in retinal detachment. *Curr Eye Res*. 2010;35:505–509.
14. Delyfer MN, Raffelsberger W, Mercier D, et al. Transcriptomic analysis of human retinal detachment reveals both inflammatory response and photoreceptor death. *PLoS One*. 2011;6:e28791.
15. Hollborn M, Francke M, Iandiev I, et al. Early activation of inflammation- and immune response-related genes after experimental detachment of the porcine retina. *Invest Ophthalmol Vis Sci*. 2008;49:1262–1273.
16. Luna G, Keeley PW, Reese BE, Linberg KA, Lewis GP, Fisher SK. Astrocyte structural reactivity and plasticity in models of retinal detachment. *Exp Eye Res*. 2016;150:4–21.
17. Matsumoto H, Kataoka K, Tsoka P, Connor KM, Miller JW, Vavvas DG. Strain difference in photoreceptor cell death after retinal detachment in mice. *Invest Ophthalmol Vis Sci*. 2014;55:4165–4174.
18. Lewis GP, Chapin EA, Luna G, Linberg KA, Fisher SK. The fate of Muller's glia following experimental retinal detachment: nuclear migration, cell division, and subretinal glial scar formation. *Mol Vis*. 2010;16:1361–1372.
19. Nakazawa T, Takeda M, Lewis GP, et al. Attenuated glial reactions and photoreceptor degeneration after retinal detachment in mice deficient in glial fibrillary acidic protein and vimentin. *Invest Ophthalmol Vis Sci*. 2007;48:2760–2768.
20. Nakazawa T, Matsubara A, Noda K, et al. Characterization of cytokine responses to retinal detachment in rats. *Mol Vis*. 2006;12:867–878.
21. Iandiev I, Uckermann O, Pannicke T, et al. Glial cell reactivity in a porcine model of retinal detachment. *Invest Ophthalmol Vis Sci*. 2006;47:2161–2171.
22. Lewis GP, Sethi CS, Carter KM, Charteris DG, Fisher SK. Microglial cell activation following retinal detachment: a comparison between species. *Mol Vis*. 2005;11:491–500.
23. Lewis G, Mervin K, Valter K, et al. Limiting the proliferation and reactivity of retinal Müller cells during experimental retinal detachment: the value of oxygen supplementation. *Am J Ophthalmol*. 1999;128:165–172.
24. Erickson PA, Fisher SK, Guerin CJ, Anderson DH, Kaska DD. Glial fibrillary acidic protein increases in Müller cells after retinal detachment. *Exp Eye Res*. 1987;44:37–48.
25. Kaneko H, Nishiguchi KM, Nakamura M, Kachi S, Terasaki H. Characteristics of bone marrow-derived microglia in the normal and injured retina. *Invest Ophthalmol Vis Sci*. 2008;49:4162–4168.
26. Pastor JC, Rojas J, Pastor-Idoate S, Di Lauro S, Gonzalez-Buendia L, Delgado-Tirado S. Proliferative vitreoretinopathy: a new concept of disease pathogenesis and practical consequences. *Prog Retin Eye Res*. 2016;51:125–155.
27. Ghodasra DH, Fante R, Gardner TW, et al. Safety and feasibility of quantitative multiplexed cytokine analysis from office-based vitreous aspiration. *Invest Ophthalmol Vis Sci*. 2016;57:3017–3023.

28. Zacks DN, Boehlke C, Richards AL, Zheng QD. Role of the Fas-signaling pathway in photoreceptor neuroprotection. *Arch Ophthalmol*. 2007;125:1389–1395.
29. Anderson DH, Guerin CJ, Erickson PA, Stern WH, Fisher SK. Morphological recovery in the reattached retina. *Invest Ophthalmol Vis Sci* 1986;27:168–183.
30. Qi Y, Dai X, Zhang H, et al. Trans-corneal subretinal injection in mice and its effect on the function and morphology of the retina. *PLoS One* 2015;10:e0136523.
31. Abcouwer SF, Lin CM, Shanmugam S, Muthusamy A, Barber AJ, Antonetti DA. Minocycline prevents retinal inflammation and vascular permeability following ischemia-reperfusion injury. *J Neuroinflammation*. 2013;10:149.
32. Liyanage SE, Gardner PJ, Ribeiro J, et al. Flow cytometric analysis of inflammatory and resident myeloid populations in mouse ocular inflammatory models. *Exp Eye Res*. 2016;151: 160–170.
33. Holladay JT. Proper method for calculating average visual acuity. *J Refract Surg*. 1997;13:388–391.
34. Chinskey ND, Besirli CG, Zacks DN. Retinal cell death and current strategies in retinal neuroprotection. *Curr Opin Ophthalmol*. 2014;25:228–233.
35. Lee JE, Liang KJ, Fariss RN, Wong WT. Ex vivo dynamic imaging of retinal microglia using time-lapse confocal microscopy. *Invest Ophthalmol Vis Sci*. 2008;49:4169–4176.
36. Takahashi S, Adachi K, Suzuki Y, Maeno A, Nakazawa M. Profiles of inflammatory cytokines in the vitreous fluid from patients with rhegmatogenous retinal detachment and their correlations with clinical features. *Biomed Res Int*. 2016; 2016:4256183.
37. Zhao Q, Ji M, Wang X. IL-10 inhibits retinal pigment epithelium cell proliferation and migration through regulation of VEGF in rhegmatogenous retinal detachment. *Mol Med Rep*. 2018;17:7301–7306.
38. Ramos MI, Tak PP, Lebre MC. FMS-like tyrosine kinase 3 ligand-dependent dendritic cells in autoimmune inflammation. *Autoimmun Rev*. 2014;13:117–124.
39. La Heij EC, Van De Waarenburg MP, Blaauwgeers HG, et al. Levels of basic fibroblast growth factor, glutamine synthetase, and interleukin-6 in subretinal fluid from patients with retinal detachment. *Am J Ophthalmol*. 2001;132:544–550.
40. Tuuminen R, Haukka J, Loukovaara S. Statins in rhegmatogenous retinal detachment are associated with low intravitreal angiopoietin-2, VEGF and MMP-2 levels, and improved visual acuity gain in vitrectomized patients. *Graefes Arch Clin Exp Ophthalmol*. 2015;253:1685–1693.
41. Yalcinbayir O, Buyukuysal RL, Gelisken O, Buyukuysal C, Can B. Amino acid and vascular endothelial growth factor levels in subretinal fluid in rhegmatogenous retinal detachment. *Mol Vis*. 2014;20:1357–1365.
42. Cassidy L, Barry P, Shaw C, Duffy J, Kennedy S. Platelet derived growth factor and fibroblast growth factor basic levels in the vitreous of patients with vitreoretinal disorders. *Br J Ophthalmol*. 1998;82:181–185.
43. Becher B, Tugues S, Greter M. GM-CSF: from growth factor to central mediator of tissue inflammation. *Immunity*. 2016;45: 963–973.
44. Bendall LJ, Bradstock KF. G-CSF: from granulopoietic stimulant to bone marrow stem cell mobilizing agent. *Cytokine Growth Factor Rev*. 2014;25:355–367.
45. Oishi A, Otani A, Sasahara M, et al. Granulocyte colony-stimulating factor protects retinal photoreceptor cells against light-induced damage. *Invest Ophthalmol Vis Sci*. 2008;49: 5629–5635.
46. Wallner S, Peters S, Pitzer C, Resch H, Bogdahn U, Schneider A. The granulocyte-colony stimulating factor has a dual role in neuronal and vascular plasticity. *Front Cell Dev Biol*. 2015;3: 48.
47. Ricker LJ, Altara R, Goezinne F, Hendrikse F, Kijlstra A, La Heij EC. Soluble apoptotic factors and adhesion molecules in rhegmatogenous retinal detachment. *Invest Ophthalmol Vis Sci*. 2011;52:4256–4262.
48. Zacks DN, Zheng QD, Han Y, Bakhru R, Miller JW. FAS-mediated apoptosis and its relation to intrinsic pathway activation in an experimental model of retinal detachment. *Invest Ophthalmol Vis Sci*. 2004;45:4563–4569.
49. Besirli CG, Chinskey ND, Zheng QD, Zacks DN. Inhibition of retinal detachment-induced apoptosis in photoreceptors by a small peptide inhibitor of the fas receptor. *Invest Ophthalmol Vis Sci*. 2010;51:2177–2184.
50. Michel J, Schwarz H. Expression of soluble CD137 correlates with activation-induced cell death of lymphocytes. *Cytokine* 2000;12:742–746.
51. Shao H, Fu Y, Liao T, et al. Anti-CD137 mAb treatment inhibits experimental autoimmune uveitis by limiting expansion and increasing apoptotic death of uveitogenic T cells. *Invest Ophthalmol Vis Sci*. 2005;46:596–603.
52. Zeng HY, Zhu XA, Zhang C, Yang LP, Wu LM, Tso MO. Identification of sequential events and factors associated with microglial activation, migration, and cytotoxicity in retinal degeneration in rd mice. *Invest Ophthalmol Vis Sci*. 2005;46: 2992–2999.
53. Natoli R, Jiao H, Barnett NL, et al. A model of progressive photo-oxidative degeneration and inflammation in the pigmented C57BL/6J mouse retina. *Exp Eye Res*. 2016;147:114–27.
54. Cross AK, Woodroofe MN. Chemokines induce migration and changes in actin polymerization in adult rat brain microglia and a human fetal microglial cell line in vitro. *J Neurosci Res*. 1999;55:17–23.
55. Ransohoff RM, El Khoury J. Microglia in health and disease. *Cold Spring Harb Perspect Biol*. 2015;8:a020560.
56. Kataoka K, Matsumoto H, Kaneko H, et al. Macrophage- and RIP3-dependent inflammasome activation exacerbates retinal detachment-induced photoreceptor cell death. *Cell Death Dis*. 2015;6:e1731.
57. Nakazawa T, Hisatomi T, Nakazawa C, et al. Monocyte chemoattractant protein 1 mediates retinal detachment-induced photoreceptor apoptosis. *Proc Natl Acad Sci U S A*. 2007;104:2425–2430.
58. Hisatomi T, Sakamoto T, Sonoda KH, et al. Clearance of apoptotic photoreceptors: elimination of apoptotic debris into the subretinal space and macrophage-mediated phagocytosis via phosphatidylserine receptor and integrin alphavbeta3. *Am J Pathol*. 2003;162:1869–1879.
59. Wang X, Miller EB, Goswami M, et al. Rapid monocyte infiltration following retinal detachment is dependent on non-canonical IL6 signaling through gp130. *J Neuroinflammation*. 2017;14:121.
60. Bennett ML, Bennett FC, Liddelow SA, et al. New tools for studying microglia in the mouse and human CNS. *Proc Natl Acad Sci U S A*. 2016;113:E1738–E1746.
61. Gabrusiewicz K, Ellert-Miklaszewska A, Lipko M, Sielska M, Frankowska M, Kaminska B. Characteristics of the alternative phenotype of microglia/macrophages and its modulation in experimental gliomas. *PLoS One*. 2011;6:e23902.
62. Sedgwick JD, Schwender S, Imrich H, Dorries R, Butcher GW, ter Meulen V. Isolation and direct characterization of resident microglial cells from the normal and inflamed central nervous system. *Proc Natl Acad Sci U S A*. 1991;88:7438–7442.
63. Aredo B, Zhang K, Chen X, Wang CX, Li T, Ufret-Vincenty RL. Differences in the distribution, phenotype and gene expression of subretinal microglia/macrophages in C57BL/6N (Crb1(rd8/rd8)) versus C57BL6/J (Crb1(wt/wt)) mice. *J Neuroinflammation*. 2015;12:6.

Investigative Ophthalmology & Visual Science